In silico identification of potential anti-monkeypox virus agents from *Hypericum sampsonii*

Phuoc Huynh[1], Ba-Hai Nguyen[2], Quan Ke Thai[3*]

[1]*Graduate University of Science and Technology, Vietnam Academy of Science and Technology, 18 Hoang Quoc Viet Street, Nghia Do Ward, Hanoi, Vietnam*
[2]*Faculty of Pharmacy, Binh Duong Medical College, 529 Le Hong Phong Street, Phu Loi Ward, Ho Chi Minh City, Vietnam*
[3]*Faculty of Natural Science Education, Saigon University, 273 An Duong Vuong Street, Cho Quan Ward, Ho Chi Minh City, Vietnam*

Received 12 March 2025; revised 15 April 2025; accepted 4 July 2025

Abstract:

Monkeypox (Mpox), an emerging zoonotic infectious disease caused by the monkeypox virus (MPXV), has become an escalating global health threat. A wave of outbreaks began in 2022 and continued into 2024. Currently, no vaccines or FDA-approved specific treatments exist for MPXV, making the discovery of effective antiviral drugs crucial. The A48R protein, a thymidylate kinase (TK), is recognised as a promising target for MPXV drug development due to its distinctive active site structure compared with the human homolog. *Hypericum sampsonii* Hance, a traditional medicinal herb from the Guttiferae family, has demonstrated various biological activities, including antiviral properties. By leveraging the natural compounds derived from *H. sampsonii*, this study aimed to identify potential inhibitors of the MPXV-TK protein. Molecular docking and dynamics simulations revealed two compounds, LTS0126561 and LTS0259892, with strong affinity for the TK active site. *In silico* pharmacokinetic and toxicological assessments indicated that both compounds are suitable candidates for oral drug development. These identified compounds provide a basis for developing antiviral agents against MPXV and other Orthopoxviruses. However, further experimental validation of these lead compounds is required to confirm their predicted antiviral activities.

Keywords: **A48R protein, *Hypericum sampsonii*, molecular docking, molecular simulations, monkeypox virus, natural compounds, thymidylate kinase.**

Classification numbers: **3.2, 3.5, 3.6**

1. Introduction

Mpox is a zoonotic infectious disease caused by the MPXV, a member of the Poxviridae family, which comprises 11 species, including Cowpox, Camelpox, Ectromelia, Vaccinia, and Variola viruses [1, 2]. Individuals infected with Mpox typically present with fever, severe headaches, myalgia, and fatigue, followed by a characteristic rash featuring various skin lesions and lymphadenopathy, which distinguishes MPXV from other Orthopoxviruses such as Smallpox, caused by the Variola virus [3, 4]. Initial cases were primarily reported in Central Africa, with the first diagnosis occurring in the Democratic Republic of the Congo in 1970 [5]. In 2022, an unusual resurgence of MPXV emerged, with cases identified in over 100 countries and more than 57,000 infections [6]. On July 23, 2022, the World Health Organization (WHO) declared a global health emergency due to Mpox. Since then, cases have been continuously reported. As of October 13, 2024, 8,540 confirmed cases, including 33 deaths, have been reported across 18 countries [7]. Currently, no specific antiviral drug has been developed to treat Mpox [8, 9]. Moreover, existing treatment strategies remain inadequate. Therefore, the development of targeted therapeutics for Mpox is of utmost importance.

Five poxvirus proteins-A48R, A50R, D13L, F13L, and I7L-have been proposed as useful targets for therapeutic interventions against Orthopoxvirus [10]. Among these, A48R has been identified as a promising drug target [10, 11]. It represents a novel druggable target by definition, as it is not currently the focus of any known drugs [11, 12]. A48R is a TK that has been characterised as forming a complex with thymidylate kinase diphosphate [13]. This protein phosphorylates thymidylate, thereby supporting DNA synthesis during the viral replication process [10, 12, 13]. Therefore, inhibition of TK activity is considered one of the key mechanisms for treating Mpox [12]. The significant structural differences between MPXV-TK and

*Corresponding author: Email: tkquan@sgu.edu.vn.

human thymidylate kinase at the active site make it an attractive target for its inhibitor, with minimal concern about interfering with human homolog function [12, 13].

Hypericum sampsonii Hance, belonging to the Hypericaceae family, is recognised as a traditional medicinal plant in various countries. The genus *Hypericum* (*Guttiferae*) comprises over 450 species distributed globally [14]. Several species of *Hypericum* have been widely used in folk medicine worldwide, such as *Hypericum perforatum L*. (commonly known as St. John's wort) [15]. In Asia, *H. sampsonii* is predominantly found in Vietnam, Myanmar, India, and China [16]. Additionally, many species of *Hypericum* have been employed in traditional or ethnomedicine in East Asia [17]. In recent years, there has been growing interest in the chemical composition and pharmacological effects of *H. sampsonii* [16]. Previous reports have revealed that *H. sampsonii* possesses various biological properties, including anti-inflammatory, analgesic, antitumour, and antiviral activities [16, 18, 19]. Furthermore, the kinase-inhibiting potential of compounds extracted from *H. sampsonii* has been identified [20, 21]. Therefore, we utilised a natural compound database in this study to identify potential compounds from *H. sampsonii* that may inhibit the MPXV-TK protein.

2. Materials and methods

2.1. Ligands collection and preparation

A total of 118 natural compounds from *H. sampsonii* were extracted from the LOTUS database [22]. Compounds that comply with Lipinski's Rule of Five were selected for further analysis. The three-dimensional (3D) structures, tautomers, and stereoisomers of the compounds were prepared using Maestro software (free software of D. E. Shaw Research group), followed by molecular optimiSation and minimiSation with OpenBabel [23] software using the MMFF94 force field and the steepest descent algorithm.

2.2. Protein preparation

The amino acid sequence of MPXV-TK was retrieved from GenBank (accession number YP_010377155.1). A homology model of MPXV-TK was constructed based on the crystal structure of Vaccinia virus TK (PDB ID: 2V54) using the SWISS-MODEL server [24]. The obtained MPXV-TK structure was refined using the HADDOCK Refinement tool [25] to determine the lowest energy structure. The quality of the TK model was assessed using the Structure Assessment tool of the SWISS-MODEL server [26]. For the docking process, hydrogen atoms were added to the TK structure, and charges were computed using the Gasteiger method in AutoDock Tools.

2.3. Molecular docking analysis

The active site of TK was previously identified, and the molecular binding site was thus established in this pocket (Fig. 1A) [13]. The docking process was conducted using AutoDock GPU ver 1.5.2 [27]. The grid box centre was defined based on the native ligand (thymidylate-5'-diphosphate - TYD) with docking coordinates set at x=1.134, y=0.748, z=1.657. The grid box size was 70×70×70 with a spacing of 0.375 Å. The docking system was configured with a population size of 250 and 1000 iterations for each ligand (*n_run*=1000). The binding conformation with the lowest free energy of binding predicted by AutoDock GPU for each ligand was recorded. Interactions between the ligand and protein were analysed using the Protein-Ligand Interaction Profiler server [28].

2.4. In silico pharmacokinetics and toxicological properties

The physicochemical and pharmacokinetic properties of the top hits were determined using the SwissADME server [29]. Toxicity properties, including hepatotoxicity, carcinogenicity, mutagenicity, and cytotoxicity, were predicted using the ProTox 3.0 server [30].

2.5. Molecular dynamics simulation

Classical molecular dynamics (MD) simulations were conducted to assess the stability of the protein-ligand complexes. MD simulations of the protein-ligand complexes were performed using the Desmond module of Schrödinger version 2023.4 (a free version of D.E. Shaw Research). Before the simulation, the protein-ligand complexes were prepared and minimised using Maestro within the OPLS force field. The simulation system was constructed by placing the protein-ligand complex in an orthorhombic box with 10×10×10 Å boundary dimensions and solvated in the SPC water model. The system was neutralised with Na^+ and Cl^- ions. A 100 ns simulation was conducted under the OPLS force field with NPT ensemble conditions set at 300 K, 1.01325 bar, and a time step of 2 fs. Default MD simulation parameters were applied, with the Coulombic interactions cutoff at 9.0 Å. Temperature coupling was maintained using the Nose-Hoover chain thermostat, while pressure was stabilised using the Martyna-Tobias-Klein barostat. Trajectories were saved every 10 ps for analysis. Post-simulation analyses included root-mean-square deviation (RMSD) and protein-ligand interaction evaluations, performed using the Simulation Interaction Diagram tool available in Desmond. RMSD was used to quantify the average displacement of a selected group of atoms over time relative to a reference frame. RMSD values were calculated as follows:

$$RMSD_x = \sqrt{\frac{1}{N}\sum_{i=1}^{N}\left(r_i'(t_x)\right) - r_i(t_{ref}))^2}$$

where: N is the number of atoms in the atom selection; t_{ref} is the reference time (typically the initial frame); $r_i'(t_x)$ is the position of atom i at time t after superimposing on t_{ref}; $r_i(t_{ref})$ is the position of atom i in the reference frame.

2.6. Binding free energy calculation

The MD simulation systems were used to calculate the binding free energy in order to evaluate the binding affinity between the protein and the ligand. Molecular mechanics energy combined with the generalised Born and surface area continuum solvation (MM/GBSA) method was applied to estimate the protein-ligand binding free energy (ΔG_{bind}) using the thermal_mmgbsa.py [31], which is available in the DESMOND software package. The free binding energy was calculated using the equation:

$$\Delta G_{bind} = E_{complex} - E_{Protein} - E_{Ligand}$$

3. Results and discussion

3.1. MPXV-TK structure assessment

The TK model of MPXV demonstrated high quality, with over 95% of residues falling within the favoured regions of the Ramachandran plot (Table 1, Fig. 1B). No outliers, bad bonds, or bad angles were observed (Table 1). The evaluation of local residue quality showed that none of the residues had a QMEANDisCo score below 0.8, confirming that all residues were correctly predicted in the structure (Fig. 1C). Structural analysis indicated that TK was constructed in a manner similar to other proteins of comparable size (Fig. 1D). The overall model quality score for TK was estimated to be 0.92±0.06 (Table 1). These results suggest that MPXV-TK is a suitable and reliable target for virtual screening.

Table 1. Structure quality of thymidylate kinase protein was calculated by Swiss server.

Measures	Structure assessment
Ramachandran favoured	95.54%
Ramachandran outliers	0%
Bad bonds	0/1665
Bad angles	0/2245
QMEANDisCo Global score	0.92±0.06

3.2. Virtual screening of H. sampsonii compounds

The natural compound models comply with Lipinski's rule of five from *H. sampsonii* and were successfully docked with the TK. The structures of the top three compounds, along with their access codes from the LOTUS database, exhibiting the highest free energy of binding predicted by AutoDock GPU, are listed in Table 2. The docking results

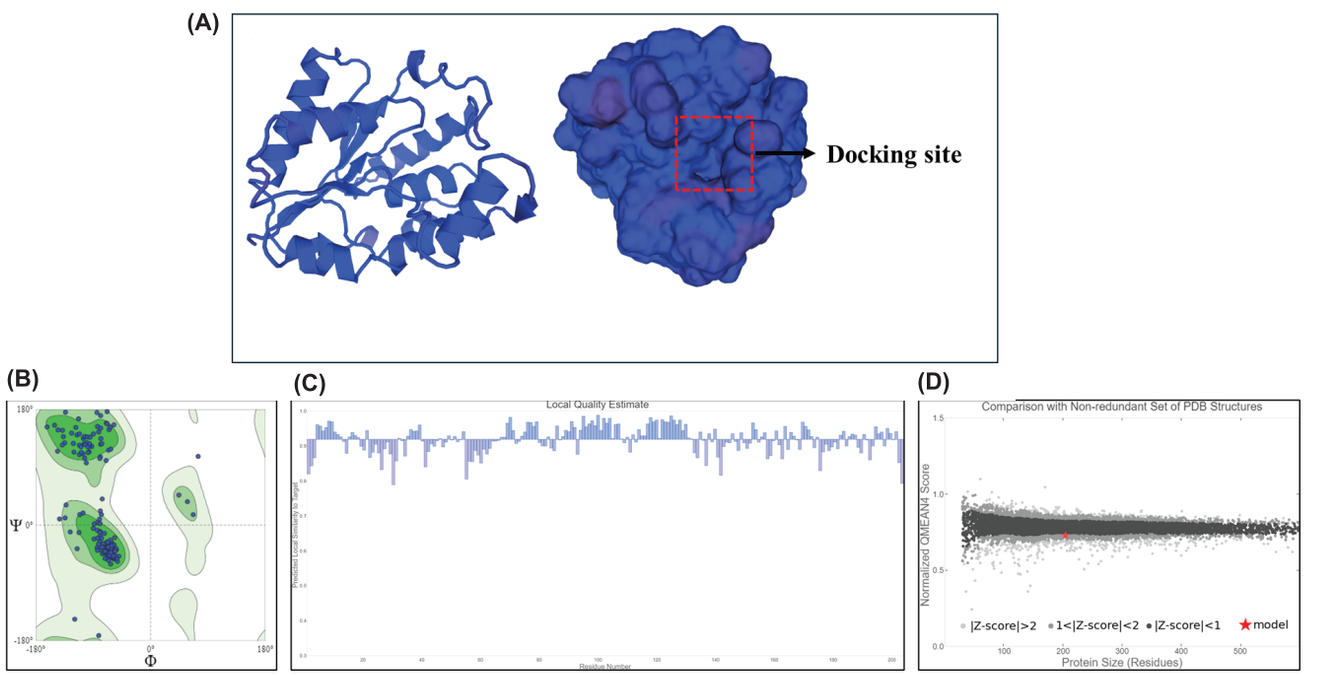

Fig. 1. Structure assessment of the Monkeypox virus thymidylate kinase protein. (A) Model of TK protein in cartoon and surface visualisation; **(B)** The Ramachandran plot; **(C)** Local quality estimate; **(D)** Comparative protein structure in the size of the same residue.

Table 2. Top three molecules obtained on virtual screening via AutoDock GPU.

No.	LOTUS ID	Structure	Free energy of binding	Chemical class	Formula
1	LTS0062524	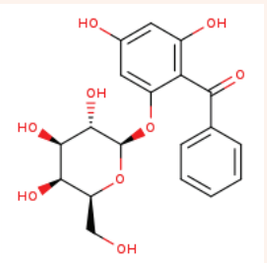	-14.36 Kcal/mol	Acyl phloroglucinols	$C_{19}H_{20}O_9$
2	LTS0126561	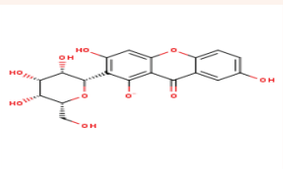	-13.86 Kcal/mol	Plant xanthones	$C_{19}H_{18}O_{10}$
3	LTS0259892	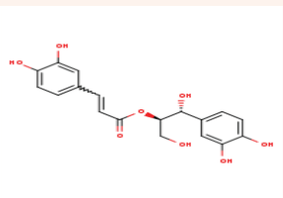	-13.49 Kcal/mol	Cinnamic acids and derivatives	$C_{18}H_{18}O_8$

Table 3. Free energy of binding and interacted residues of top three compounds docked via AutoDock GPU.

Compounds	Free energy of binding	Hydrophobic interactions	Hydrogen bonds	π-Stacking	π-Cation interactions	Salt bridges
Native ligand (TYD)	-7.29 (Kcal/mol)	Phe38, Phe68, Arg93 (Total interactions: 4)	Asp13, Lys14, Arg72, Ser97 (Total interactions: 5)	-	-	Lys14, Lys17, Arg93 (Total interactions: 4)
LTS0062524	-14.36 (Kcal/mol)	Phe38, Leu53, Phe68, Arg93 (Total interactions: 5)	Phe38, Asn65, Arg72, Tyr94, Gly98, Lys105, Tyr144 (Total interactions: 9)	Tyr144 (Total interaction: 1)	-	Arg72 (Total interaction: 1)
LTS0126561	-13.86 (Kcal/mol)	Tyr101, Tyr144 (Total interactions: 3)	Asn65, Arg72, Gly98, Tyr101, Lys105, Glu142, Tyr144 (Total interactions: 9)	Phe68 (Total interaction: 1)	Arg93 (Total interaction: 1)	-
LTS0259892	-13.49 (Kcal/mol)	Phe68, Tyr101 (Total interactions: 4)	Lys17, Asn37, Arg41, Asn65, Asp92, Tyr101, Lys105, Glu142, Tyr144 (Total interactions: 11)	Phe68 (Total interaction: 1)	-	Arg93 (Total interaction: 1)

indicated that all three ligands were positioned correctly within the predicted binding site and displayed stronger affinities than the native ligand - TYD (Table 2). Interaction analyses between the protein and ligands revealed that all three compounds formed interactions with key residues in the pocket: Asp13, Lys14, Lys17, Phe38, Arg41, Phe68, Arg72, Arg93, Ser97, Lys105, Glu142, and Tyr144 (Table 2). Notably, the three ligands formed more hydrogen bonds than TYD and established two additional characteristic interactions: π-stacking and π-cation interactions (Fig. 2, Table 3). The formation of a hydrogen bond with Lys105 of TK is particularly significant, as this residue contributes to the differences in the active site between the TK of MPXV and that of humans. Furthermore, interactions with Asp13, Lys17, and Arg41 are crucial for TK inhibition, as these amino acids are involved in substrate catalysis within the protein. Table 3 and Fig. 2 detail and analyse the interactions and binding models.

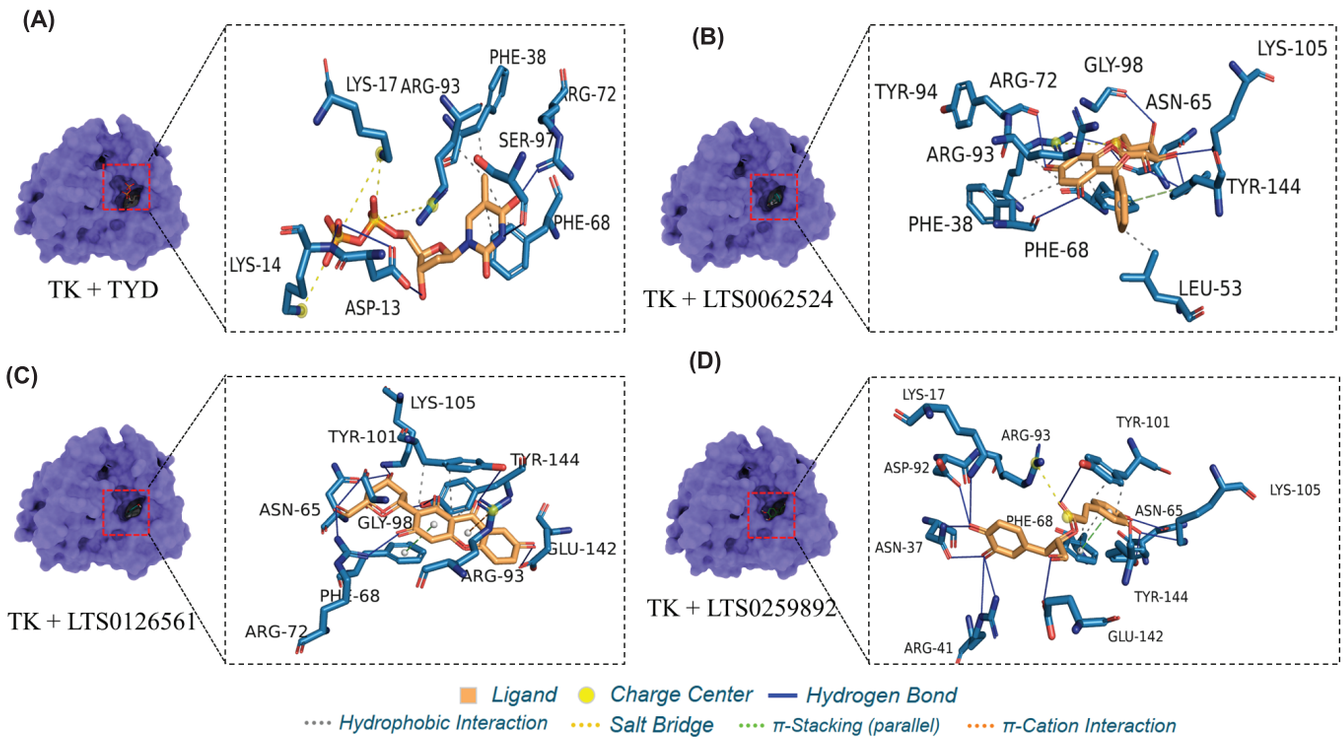

Fig. 2. 3D interactions of the top three compounds in the active site of thymidylate kinase protein. Each panel displays for each 3D interaction between ligand and Thymidylate kinase of MPXV. Types of interaction were presented in dashline. **(A)** Thymidylate kinase + TYD; **(B)** Thymidylate kinase + LTS0062524; **(C)** Thymidylate kinase + LTS0126561; **(D)** Thymidylate kinase + LTS0259892.

Table 4. Drug likeness property analysis of top three compounds by SwissADME prediction.

Drug likeness property	LTS0062524	LTS0126561	LTS0259892
Formula	$C_{19}H_{20}O_9$	$C_{19}H_{17}O_{10}$	$C_{18}H_{18}O_8$
Molecular weight	392.36 g/mol	405.33 g/mol	362.33 g/mol
Number of heavy atoms	28	29	26
Number of aromatic heavy atoms	12	14	12
Number of rotatable bonds	5	2	7
Number of H-bond acceptor	9	10	8
Number of H-bond donor	6	6	6
Molar refractivity	94.51	96.79	91.95
LogP	-0.16	-0.36	0.96
TPSA	156.91 Å²	183.88 Å²	147.68 Å²
Lipinski's rule of five	Yes	Yes	Yes
BBB permeant	No	No	No
Water solubility	Soluble	Soluble	Soluble
Bioavailability score	0.55	0.11	0.55

3.3. In silico pharmacokinetics and toxicological properties

The drug-likeness of the top three compounds was assessed using Lipinski's Rule of Five and SwissADME parameters. The physicochemical properties of these compounds are listed in Table 4. All three compounds comply with Lipinski's Rule of Five and exhibit water solubility. The analysis results indicate good oral bioavailability for these compounds due to their favourable water solubility and acceptable bioavailability scores (Table 4, Fig. 3).

The toxicity profiles of the three compounds were predicted using ProTox 3.0. The findings from the toxicological predictions revealed that these compounds are non-hepatotoxic, non-carcinogenic, non-mutagenic, and non-cytotoxic, with acceptable LD_{50} values indicating a high reliability of the predictions. However, it is important to note that compound LTS0126561 has an LD_{50} of 2 mg/kg, warranting caution in clinical trials.

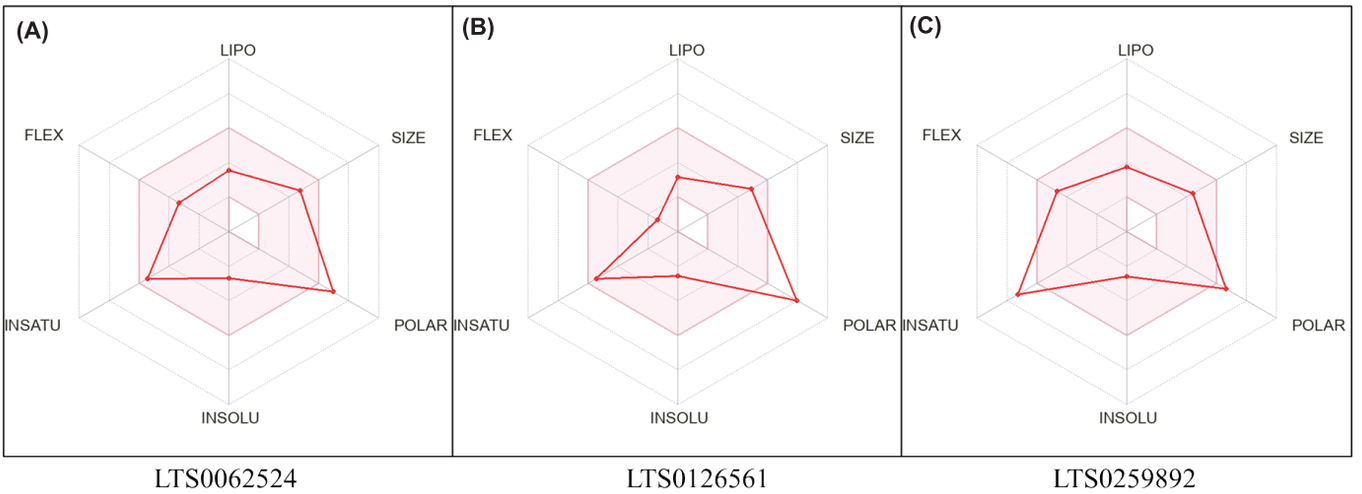

Fig. 3. Oral bioavailability of three compounds were predicted by SwissADME. Each picture displayed for each compound as **(A)** LTS0062524, **(B)** LTS0126561, **(C)** LTS0259892. The colour zone represents the physiochemical space for oral bioavailability. LIPO (lipophilicity): -0.7<XLOGP3<+5.0; SIZE: <500g/mol; POLAR (Polarity): 20Å²<TPSA<130Å²; INSOLU (Insolubility) -6<LogS (ESOL)<0; INSATU (Instauration): 0.25<fraction Csp^3<1; FLEX (Flexibility): 0<Num. rotatable bonds<9.

Table 5. Toxicity prediction of top three compounds.

Toxicity prediction	LTS0062524	LTS0126561	LTS0259892
Hepatotoxicity (Probability)	Inactive (85%)	Inactive (80%)	Inactive (79%)
Cardiotoxicity (Probability)	Active (66%)	Inactive (63%)	Inactive (56%)
Carcinogenicity (Probability)	Inactive (77%)	Inactive (71%)	Inactive (77%)
Mutagenicity (Probability)	Inactive (79%)	Inactive (50%)	Inactive (81%)
Cytotoxicity (Probability)	Inactive (85%)	Inactive (86%)	Inactive (91%)
Predicted LD_{50}	2000 mg/kg	2 mg/kg	5000 mg/kg

3.4. Molecular dynamics simulations

Molecular dynamics simulations provide valuable insights into the conformational changes of compounds when they bind to the active site of the TK. Based on the docking scores and interactions, the top three compounds mentioned previously underwent MD simulations. We analysed the RMSD values of the TK while binding with different ligands (Fig. 4A). The results revealed variations in the oscillations of the TK protein when interacting with compounds LTS0062524 and LTS0126561. Both exhibited higher RMSD values compared to TYD, which had recorded values of 0.22±0.03, 0.19±0.03, and 0.14±0.02 nm, respectively. Previous studies have documented similar changes in the RMSD of the protein when interacting with different ligands [8, 32]. This is believed to occur because the protein must alter its initial conformation to interact with the new ligand stably. In contrast, the fluctuations of the TK protein when binding with compound LTS0259892 were comparable to those observed with TYD, yielding an RMSD of 0.14±0.01 nm. No unusual protein fluctuations were detected during the simulations, indicating that the protein structure remained stable throughout the entire simulation process.

The stability of the compounds' binding to the pocket of the TK during simulations is illustrated by the RMSD of the ligands fitting on the protein (Fig. 4B). Overall, in all simulations, the ligands maintained binding within the pocket, with no instances of ligands moving out of the active site of the TK protein. Compared to the positions predicted by docking, the MD simulation results indicate that compound LTS0062524 remained stable only from 0 to 20 ns of simulation, after which it exhibited significant fluctuations within the pocket of the TK before unhurriedly stabilising again (Fig. 4B). Compounds LTS0126561 and LTS0259892 showed comparable stability in their interactions within the pocket to that of TYD. Notably, compound LTS0126561 remained very stable for the first 50 ns of the simulation, followed by strong fluctuations from 50 to 70 ns, after which it stabilised for the remainder of the simulation (Fig. 4B). In contrast, compound LTS0259892 demonstrated greater fluctuations than TYD in the early stages of the simulation, but after 60 ns, it showed reduced oscillations and maintained a stability level similar to TYD (Fig. 4B). In general, the average RMSD values recorded for the three compounds LTS0062524, LTS0126561, and LTS0259892 were acceptable, measuring 0.37±0.11, 0.20±0.13, and 0.32±0.04 nm, respectively.

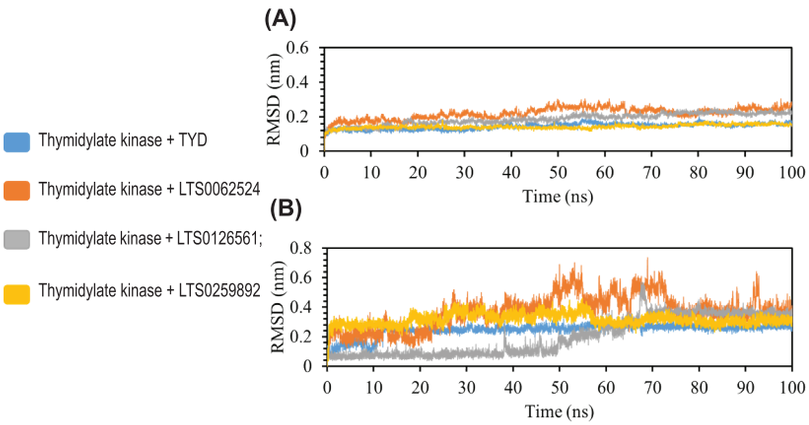

Fig. 4. Root-mean-square deviation (RMSD) of protein and ligands in molecular dynamics simulation. (A) RMSD of TK protein in complex with difference ligands; **(B)** RMSD of each ligand fit on TK protein. Each colour displays for each complex: Blue: Thymidylate kinase + TYD; Orange: Thymidylate kinase + LTS0062524; Grey: Thymidylate kinase + LTS0126561; Yellow: Thymidylate kinase + LTS0259892.

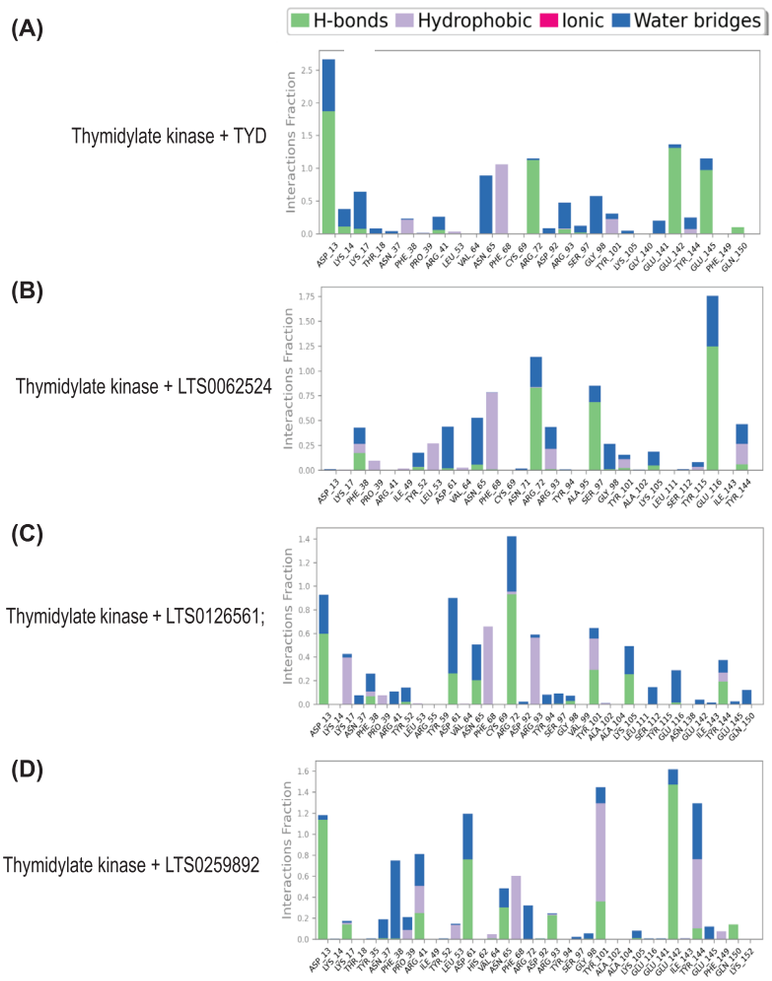

Fig. 5. Protein-ligand contacts analysis of TYD and *H. sampsonii* compounds. Each panel displays interaction between ligand and thymidylate kinase. (A) Thymidylate kinase + TYD; **(B)** Thymidylate kinase + LTS0062524; **(C)** Thymidylate kinase + LTS0126561; **(D)** Thymidylate kinase + LTS0259892. Each colour displays for each interaction type: Green: Hydrogen bond; Grey: Hydrophobic; Red: Ionic; Blue: Water bridges.

The stability of the compounds' binding to the residues of TK was analysed. The results indicate that compounds LTS0126561 and LTS0259892 formed a more diverse array of interactions compared to TYD (Fig. 5). In contrast, compound LTS0062524 exhibited weaker interactions with the residues within the pocket, which partly explains its significant fluctuations during the simulation. TYD primarily formed hydrogen bonds with residues Asp13, Arg72, Glu142, and Glu145, as well as water bridges with residues Asp13, Lys17, Asn65, Arg93, and Gly98. In comparison, the two compounds (LTS0126561 and LTS0259892) not only maintained stable hydrogen bonds with residues Asp13, Arg72, and Glu142 but also established additional hydrogen bonds with residues Asp61, Asn65, Tyr101, and Glu142 (Fig. 5). Among the interactions in the protein-ligand complex, water bridges, ionic interactions, hydrophobic interactions, and hydrogen bonding were the most characteristic types [33]. Hydrogen bonds are crucial in drug design and development [33]. Therefore, the formation of multiple stable hydrogen bonds enhances the drug development potential of these two compounds. Hydrophobic interactions and water bridges with the TK protein were also noted for compounds LTS0126561 and LTS0259892.

Binding affinity reflects the strong interaction between a compound and a protein through binding free energy measure (ΔG_{bind}). Based on the simulation results, the last 20 ns were sampled to estimate the binding free energy (ΔG_{bind}) using the MM/GBSA method (Fig. 6). The analysis revealed that the binding affinity of compound LTS0062524 with the TK protein was (ΔG_{bind})=-43.39±3.52 Kcal/mol, which is weaker than that of TYD, with (ΔG_{bind})=-59.34±3.69 Kcal/mol (Fig. 6). This indicates that compound LTS0062524 is less effective in binding to the active site of the TK protein. In contrast, compounds LTS0126561 and LTS0259892 demonstrated stronger affinities than TYD, with recorded ΔG_{bind} values of -67.12±5.18 and -62.70±4.73 Kcal/mol, respectively. This suggests that these two compounds have a strong potential for binding effectively to the active site of TK, thereby inhibiting the kinase activity of this protein.

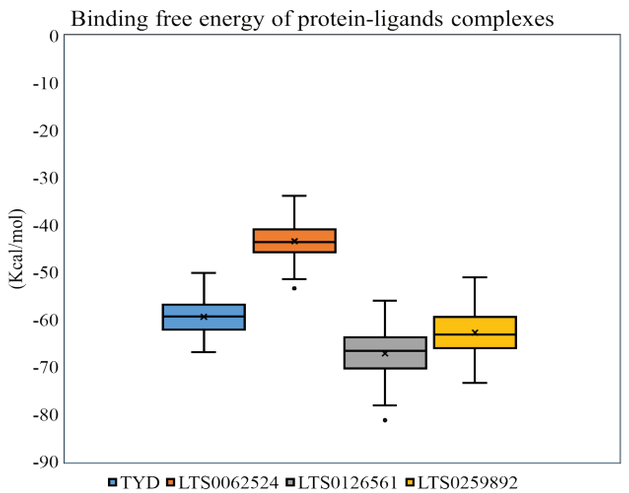

Fig. 6. The binding free energy of protein-ligand complexes. Molecular mechanics with generalised Born surface area solvation results for all the complexes. All the energies are given in Kcal/mol. Each colour displays for each complex: Blue: Thymidylate kinase + TYD; Orange: Thymidylate kinase + LTS0062524; Grey: Thymidylate kinase + LTS0126561; Yellow: Thymidylate kinase + LTS0259892.

The structural differences in the TK between humans and the MPXV make this protein a promising target for drug development. The lack of specific therapeutic options for Mpox raises concerns about the potential global spread of the disease. Using existing smallpox treatments, such as tecovirimat, cidofovir, or brincidofovir, is met with scepticism due to experimental models [12] and the absence of appropriate treatment protocols [9, 11]. Consequently, there is an urgent need to develop drugs that can specifically inhibit MPXV. Traditional drug development methods are often time-consuming, but employing *in silico* analysis techniques can accelerate the screening of potential compounds. Additionally, plants are a valuable source of medicinal materials for developing new drug molecules. As a result, virtual screening studies of natural compounds derived from plants using molecular docking and MD simulations are becoming increasingly common and play an essential role in developing virus inhibitors. A notable example is the identification of the inhibitor N3 for the main protease (Mpro) of SARS-CoV-2 through virtual screening [34]. The potential and drug-like characteristics of any compound can be assessed through its binding efficacy, stability, and toxicity [35]. We have identified two compounds, LTS0126561 and LTS0259892, that show promise in inhibiting the active site of the TK protein. Upon retrieving data from the LOTUS database, we have found that these two compounds are exclusive to the species *H. sampsonii* and are not present in other species within the *Hypericum* genus. Analyses of toxicity and drug-likeness indicate that LTS0126561 and LTS0259892 are potential candidates for oral drug development. This study highlights a promising pathway for developing targeted therapies against MPXV. The identified compounds should be further evaluated to confirm their efficacy against MPXV *in vitro*. These compounds could serve as a framework for MPXV drug design and lead optimisation in the future.

4. Conclusions

Molecular docking results and MD simulations have identified two notable natural compounds from *H. sampsonii* with strong affinity for the thymidylate kinase of MPXV: LTS0126561 and LTS0259892 in the LOTUS database. *In silico* analyses of pharmacokinetic and toxicological properties indicate that these compounds are suitable for development as oral molecules. Therefore, these compounds hold promise as potential antiviral agents against MPXV by inhibiting the active site of thymidylate kinase. However, it is essential to extend the simulations and conduct comprehensive *in vitro*, *in vivo*, and preclinical studies to determine the efficacy of these compounds as antiviral drugs.

CRediT author statement

Phuoc Huynh: Methodology, Formal analysis, Original draft preparation, Visualisation, Investigation, Supervision, Validation, Writing - Reviewing and Editing; Ba-Hai Nguyen: Conceptualisation, Data curation, Investigation, Supervision, Validation, Writing - Reviewing and Editing; Quan Ke Thai: Methodology, Formal analysis, Original draft preparation, Visualisation, Investigation, Supervision, Validation, Writing - Reviewing and Editing

COMPETING INTERESTS

The authors declare that there is no conflict of interest regarding the publication of this article.

REFERENCES

[1] G. Preet, E.T. Oluwabusola, B.F. Milne, et al. (2022), "Computational repurposing of mitoxantrone-related structures against monkeypox virus: A molecular docking and 3D pharmacophore study", *Int. J. Mol. Sci.*, **23**, DOI: 10.3390/ijms232214287.

[2] J. Kaler, A. Hussain, G. Flores, et al. (2022), "Monkeypox: A comprehensive review of transmission, pathogenesis, and manifestation", *Cureus*, **14**, DOI: 10.7759/cureus.26531.

[3] N.V. Kandra, A.M. Varghese, P.K. Uppala, et al. (2023), "Monkeypox outbreak in the post-eradication era of smallpox", *Egypt J. Intern. Med.*, **35**, DOI: 10.1186/s43162-023-00196-2.

[4] E. Lansiaux, N. Jain, S. Laivacuma, et al. (2022), "The virology of human monkeypox virus (hMPXV): A brief overview", *Virus Research*, **322**, DOI: 10.1016/j.virusres.2022.198932.

[5] E.M. Bunge, B. Hoet, L. Chen, et al. (2022), "The changing epidemiology of human monkeypox - A potential threat? A systematic review", *PLOS Negl. Trop. Dis.*, **16**, DOI: 10.1371/journal.pntd.0010141.

[6] Q. Gong, C. Wang, X. Chuai, et al. (2022), "Monkeypox virus: A re-emergent threat to humans", *Virol. Sin.*, **37**, pp.477-482, DOI: 10.1016/j.virs.2022.07.006.

[7] World Health Organization (2024), *Mpox Outbreak: Global Trends*, https://worldhealthorg.shinyapps.io/mpx_global/, accessed 22 October 2024.

[8] T.T.D. Pham, Q.M. Thai, P.N.K. Tuyen, et al. (2024), "Computational discovery of tripeptide inhibitors targeting monkeypox virus A42R profilin-like protein", *J. Mol. Graph.*, **132**, DOI: 10.1016/j.jmgm.2024.108837.

[9] M. Amjid, M.M. Khan, S.F. Pastore, et al. (2024), "Identification of antiviral drug candidates against monkeypox DNA polymerase and profilin-like protein A42R utilizing an *in-silico* approach", *bioRxiv*, DOI: 10.1101/2024.08.15.608157.

[10] M.N. Prichard, E.R. Kern (2012), "Orthopoxvirus targets for the development of new antiviral agents", *Antiviral. Res.*, **94**, pp.111-125, DOI: 10.1016/j.antiviral.2012.02.012.

[11] M. Pourhajibagher, A. Bahador (2023), "Virtual screening and computational simulation analysis of antimicrobial photodynamic therapy using propolis-benzofuran A to control of Monkeypox", *Photodiagnosis Photodyn. Ther.*, **41**, DOI: 10.1016/j.pdpdt.2022.103208.

[12] H.Y.I. Lam, J.S. Guan, Y. Mu (2022), "*In silico* repurposed drugs against monkeypox virus", *Molecules*, **27**, DOI: 10.3390/molecules27165277.

[13] C. Caillat, D. Topalis, L.A. Agrofoglio, et al. (2008), "Crystal structure of poxvirus thymidylate kinase: An unexpected dimerization has implications for antiviral therapy", *Proc. Natl. Acad. Sci.*, **105**, pp.16900-16905, DOI: 10.1073/pnas.0804525105.

[14] A. Karioti, A.R. Bilia (2010), "Hypericins as potential leads for new therapeutics", *Int. J. Mol. Sci.*, **11**, pp.562-594, DOI: 10.3390/ijms11020562.

[15] G. Stojanović, A. Đorđević, A. Šmelcerović (2013), "Do other *Hypericum* species have medical potential as St. John's wort (*Hypericum perforatum*)?", *Curr. Med. Chem.*, **20**, pp.2273-2295, DOI: 10.2174/0929867311320180001.

[16] Z. Sun, Y. Li, R. Zhong, et al. (2023), "*Hypericum sampsonii* Hance: A review of its botany, traditional uses, phytochemistry, biological activity, and safety", *Front. Pharmacol.*, **14**, DOI: 10.3389/fphar.2023.1247675.

[17] R. Zhang, Y. Ji, X. Zhang, et al. (2020), "Ethnopharmacology of *Hypericum* species in China: A comprehensive review on ethnobotany, phytochemistry and pharmacology", *J. Ethnopharmacol.*, **254**, DOI: 10.1016/j.jep.2020.112686.

[18] J. Zhang, L. Gao, J. Hu, et al. (2022), "Hypericin: Source, determination, separation, and properties", *Sep. Purif. Rev.*, **51**, pp.1-10, DOI: 10.1080/15422119.2020.1797792.

[19] Y.L. Lin, Y.S. Wu (2003), "Polyprenylated phloroglucinol derivatives from *Hypericum sampsonii*", *Helv. Chim. Acta.*, **86**, pp.2156-2163, DOI: 10.1002/hlca.200390173.

[20] I. Takahashi, S. Nakanishi, E. Kobayashi, et al. (1989), "Hypericin and pseudohypericin specifically inhibit protein kinase C: Possible relation to their antiretroviral activity", *Biochem. Biophys. Res. Commun.*, **165**, pp.1207-1212, DOI: 10.1016/0006-291X(89)92730-7.

[21] T.K. Quan, H. Phuoc, H.B.T. Hai, et al. (2024), "*In silico* evaluation of hypericin and pseudohypericin as candidates for monkeypox treatment", *Vietnam J. Biotechnol.*, **22**, pp.79-89, DOI: 10.15625/vjbt-20641.

[22] A. Rutz, M. Sorokina, J. Galgonek, et al. (2022), "The LOTUS initiative for open knowledge management in natural products research", *eLife*, **11**, DOI: 10.7554/eLife.70780.

[23] N.M. O'Boyle, M. Banck, C.A. James, et al. (2011), "Open Babel: An open chemical toolbox", *J. Cheminformatics*, **3**, DOI: 10.1186/1758-2946-3-33.

[24] A. Waterhouse, M. Bertoni, S. Bienert, et al. (2018), "SWISS-MODEL: Homology modelling of protein structures and complexes", *Nucleic Acids Res.*, **46**, pp.W296-W303, DOI: 10.1093/nar/gky427.

[25] T. Neijenhuis, S.C. Keulen, A.M.J.J. Bonvin (2022), "Interface refinement of low- to medium-resolution Cryo-EM complexes using HADDOCK2.4", *Structure*, **30**, pp.476-484, DOI: 10.1016/j.str.2022.02.001.

[26] A.M. Waterhouse, G. Studer, X. Robin, et al. (2024), "The structure assessment web server: For proteins, complexes and more", *Nucleic Acids Res.*, **52**, pp.318-323, DOI: 10.1093/nar/gkae270.

[27] D. Santos-Martins, L. Solis-Vasquez, A.F. Tillack, et al. (2021), "Accelerating AutoDock4 with GPUs and gradient-based local search", *J. Chem. Theory Comput.*, **17**, pp.1060-1073, DOI: 10.1021/acs.jctc.0c01006.

[28] M.F. Adasme, K.L. Linnemann, S.N. Bolz, et al. (2021), "PLIP 2021: Expanding the scope of the protein-ligand interaction profiler to DNA and RNA", *Nucleic Acids Res.*, **49**, pp.W530-W534, DOI: 10.1093/nar/gkab294.

[29] A. Daina, O. Michielin, V. Zoete (2017), "SwissADME: A free web tool to evaluate pharmacokinetics, drug-likeness and medicinal chemistry friendliness of small molecules", *Sci. Rep.*, **7**, DOI: 10.1038/srep42717.

[30] P. Banerjee, E. Kemmler, M. Dunkel, et al. (2024), "ProTox 3.0: A webserver for the prediction of toxicity of chemicals", *Nucleic Acids Res.*, **52**, pp.513-520, DOI: 10.1093/nar/gkae303.

[31] J. Li, R. Abel, K. Zhu, et al. (2011), "The VSGB 2.0 model: A next generation energy model for high resolution protein structure modeling", *Proteins*, **79**, pp.2794-2812, DOI: 10.1002/prot.23106.

[32] M. Hassam, M.A. Bashir, S. Shafi, et al. (2022), "Identification of potent compounds against SARs-CoV-2: An *in-silico* based drug searching against Mpro", *Comput. Biol. Med.*, **151**, DOI: 10.1016/j.compbiomed.2022.106284.

[33] R.K. Mohapatra, A. Mahal, P.K. Mohapatra, et al. (2024), "Structure-based discovery of *F. religiosa* phytochemicals as potential inhibitors against Monkeypox (Mpox) viral protein", *J. Biosaf. Biosecur.*, **6**, pp.157-169, DOI: 10.1016/j.jobb.2024.05.004.

[34] Z. Jin, X. Du, Y. Xu, et al. (2020), "Structure of Mpro from SARS-CoV-2 and discovery of its inhibitors", *Nature*, **582**, pp.289-293, DOI: 10.1038/s41586-020-2223-y.

[35] A.B. Raies, V.B. Bajic (2016), "*In silico* toxicology: Computational methods for the prediction of chemical toxicity", *Wiley Interdiscip. Rev. Comput. Mol. Sci.*, **6**, pp.147-172, DOI: 10.1002/wcms.1240.